DOI: 10.13009/EUCASS2019-510

DOI:

Design of the trajectory of a tether mission to Saturn

Riccardo Calaon[⋆], *Elena Fantino*[§], *Roberto Flores* [‡] *and Jesús Peláez*[†]
[⋆]*Dept. of Industrial Engineering, University of Padova*
Via Gradenigio G/a -35131- Padova, Italy
[§]*Dept. of Aerospace Engineering, Khalifa University*
Abu Dhabi, Unites Arab Emirates
[‡]*Inter. Center for Numerical Methods in Engineering*
Campus Norte UPC, Gran Capitán s/n, Barcelona, Spain
[†]*Space Dynamics Group, UPM*
School of Aeronautical and Space Engineering, Pz. Cardenal Cisneros 3, Madrid, Spain
riccardo.calaon.1@studenti.unipd.it, elena.fantino@ku.ac.ae, rflores@cimne.upc.edu, j.pelaez@upm.es
[†]Corresponding author

Abstract

This paper faces the design of the trajectory of a tether mission to Saturn. To reduce the hyperbolic excess velocity at arrival to the planet, a gravity assist at Jupiter is included. The Earth-to-Jupiter portion of the transfer is unpropelled. The Jupiter-to-Saturn trajectory has two parts: a first coasting arc followed by a second arc where a low thrust engine is switched on. An optimization process provides the law of thrust control that minimizes the velocity relative to Saturn at arrival, thus facilitating the tethered orbit insertion.

1. Introduction

The outer planets are of particular interest in terms of what they can reveal about the origin and evolution of our solar system. They are also local analogues for the many extra-solar planets that have been detected over the past twenty years. The study of these planets furthers our comprehension of our neighbourhood and provides the foundations to understand distant planetary systems. The giant planet satellites have their own special place in our quest for learning about our origins and our search for life, and robotic missions are essential tools for this scientific goal. As an example, exploring the moons of *Saturn*, particularly *Enceladus*, is an important goal of planetary science, the more so for search of life outside the Earth. As a consequence, missions to the outer planets have been prioritized by NASA and ESA, and this has resulted in important space projects for the exploration of the Jupiter's system, such as NASA's Europa Clipper spacecraft[12] and the ESA's Jupiter Icy Moons Explorer.[13]

The visit to the neighborhood of a Giant Planet (Ice or Gas) requires that the S/C be decelerated and captured by planets' gravity upon arrival from an interplanetary trajectory. In fact, insertion into orbit around any outer planet is highly demanding in terms of propellant. Cassini/Huygens travelled to Saturn following a ΔV-VVEJGA trajectory. Then, in order to capture the S/C, a Saturn Orbit Insertion (SOI) manoeuver was performed with a bipropellant engine which produced a velocity variation of 622 m/s and burnt approximately 800 kg of fuel.[1,3] The impact of an impulsive OI manoeuver on the mass budget and eventually on the size and overall cost of the mission is high.

Note that no mission to Uranus or Neptune —similar to the Cassini/Huygens— has ever been undertaken due to the prohibitive amount of propellant required in the OI manoeuver. However, as regarding the scientific exploration of Giant Planets, an interesting option can be found in the *Electrodynamic Tether* (ET) concept. In particular, the bare self-balanced electrodynamic tether concept[4] could play a significative role in this field because it makes it possible to capture the S/C using a conductive tether.

When an ET is used for the capture, a paramount parameter is the *capture efficiency*, defined as the ratio $M_{S/C}/m_t$, that is, is the S/C-to-tether mass ratio. Whereas use of ET's is readily possible for Jupiter,[15] the case for the other three Outer Giant Planets, Saturn, Uranus and Neptune, presents issues, basically because their magnetic self-field $\mathbf{B}$ is grossly weaker (the efficiency of spacecraft capture with an ET goes down as B^2).

But even the most distant planets can be visited exploiting the characteristics of ET's. Recently (see reference[21]) the tether-assisted capture of a probe by Neptune has been considered showing that the *capture efficiency* can be reach values of the order of 12. This preliminary analysis shows that using ET's in a mission to Neptune provide similar efficiencies than in Jupiter[8] or in Saturn.[17]

DOI: 10.13009/EUCASS2019-510

The analysis carried out in this paper focuses on Saturn, but an important part of it can be extended to the other Giant Planets. Considering the Saturn case, however, if the relative velocity between the S/C and Saturn at the encounter is sufficiently decreased, the capture of the probe can be performed in a reliable way by using the electrodynamic drag provided by the ET (see reference 17).

The ET concept open the door to a *minor mission* to explore Saturn and its moons with masses below the ton (the mass of the Cassini/Huygens spacecraft at launch pad was about 5,600 kg). This fact makes easy the design of the interplanetary trajectory that leads to the world of Saturn due to the lower value of the launch energy C_3. The influence of the C_3 parameter on the maneuver has been studied in detail in other communication presented at this conference[20] and in a previous paper.[19]

The benefit of decreasing hyperbolic excess velocity in the encounter with Saturn turns out to be important for several reasons. The present contribution is a feasibility study of a strategy to minimize the hyperbolic excess speed upon arrival at Saturn and thus the amount of propellant required for the SOI manoeuver, with a consequent larger available payload mass fraction.

The analysis focuses on the combined use of two *tools* available in interplanetary missions: 1) a gravity assist in Jupiter, and 2) an optimization of a low thrust trajectory at the Saturn arrival. A more detailed analysis of some parts of this paper can be found in.[18]

This article is the result of the joint effort of two research groups, at the Khalifa University and the Polytechnic University of Madrid.

1.1 Proposed approach and preliminary results

Some preliminary solutions where calculated as a base for further analysis for this work. In both cases, the mission consisted in reaching Saturn performing a planetary flyby around Jupiter, to increase the spacecraft's semi-major axis and reduce the relative speed at the encounter with Saturn. The two solutions presented were calculated with the MGA (multiple gravity assist) strategy; no constraints were added to the computation, as the results were to be further processed in the following sections of this work. The planetary ephemerides were calculated from the planets' state vectors at a given time, *after removing out-of-plane components in order to obtain planar orbits.* The keplerian parameters are therefore affected by inaccuracies, and do not account for secular variations which, in a final analysis, should be taken into account given the long times involved in the mission. This will not affect the validity of the calculations carried out subsequently, as they would only need to be corrected with the real planetary ephemerides. The two solution only differ in the way the cost function was formulated: in the first case a global optimum solution is searched, accounting for the total cost of launch, maneuver and planetary capture; in the secondo case, only the maneuver $\Delta \boldsymbol{v}$ is minimized, resulting in a free Jupiter flyby. The details of the optimization process can be found in.[18]

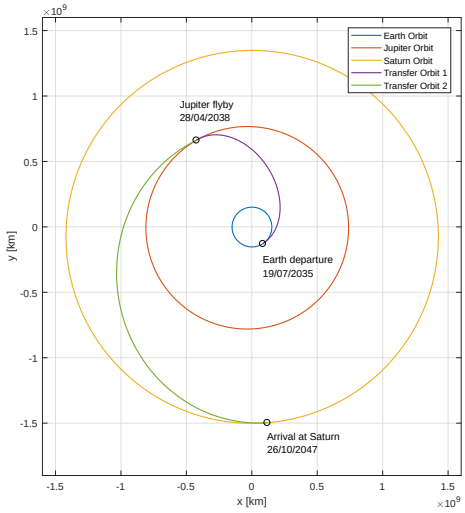

Figure 1: First optimized trajectory

1.2 First case: global optimization

In this case the global impulse

$$\Delta \boldsymbol{v}_{tot} = \Delta \boldsymbol{v}_{launch} + \Delta \boldsymbol{v}_{fb} + \boldsymbol{v}_{\infty,S}$$

is optimized including the impulse $\boldsymbol{v}_{fb}$ imparted in the Jupiter flyby. The current orbit sequence is obtained with the following $\Delta \boldsymbol{v}'s$:

- $\Delta \boldsymbol{v}_{launch} = 6.304$ km/s;
- $\Delta \boldsymbol{v}_{fb} = -0.3584$ km/s (fired against the spacecraft's speed);
- $\boldsymbol{v}_{\infty,S} = 1.4245$ km/s.

The flyby has its close approach to Jupiter in 205871 km. Table 1 summarizes the most significative parameters.

DOI: 10.13009/EUCASS2019-510

Table 1: First trajectory (Figure 1)

	Earth	Jupiter	Saturn	Transfer 1	Transfer 2
Encounter date	19/07/2035	28/04/2038	26/10/2047		
e	0.01136	0.04589	0.05377	0.6729	0.3246
ω (deg)	130.100	11.4535	92.003	302.745	96.2015
θ (rad)	3.0177	1.9407	3.185		
a (km)	1.5194e08	7.7453e08	1.425e09		
$\theta_{\text{departure}}$ (rad)				0.00445	0.46159
θ_{arrival} (rad)				3.1399	3.1117
ΔT (years)				2.78	9.50

Table 2: Second trajectory (Figure 2)

	Earth	Jupiter	Saturn	Transfer 1	Transfer 2	Flyby Orbit
Encounter date	13/10/2037	23/03/2040	19/02/2047			
e	0.01136	0.04589	0.05377	0.6880	0.4553	1.6851
ω (deg)	130.100	11.4535	92.003	5.2134	88.6728	147.244[2]
θ (rad)	4.1776	2.8938	3.0540			
a (km)	1.5194e08	7.7453e08	1.425e09			
$\theta_{\text{departure}}$ (rad)				0.07414	1.54606	/
θ_{arrival} (rad)				3.0027	3.1121	/
ΔT (years)				2.44	6.91	/
r_P (km)				/	/	2.7072e06

1.3 Second case: pure flyby

In this case $\boldsymbol{v}_{fb} = 0$. The current orbit sequence is obtained with the following $\Delta\boldsymbol{v}$'s:

- $\Delta\boldsymbol{v}_{launch} = 6.435$ km/s;
- $\Delta\boldsymbol{v}_{fb} = 6.08 \cdot 10^{-12}$ km/s;
- $\boldsymbol{v}_{\infty,S} = 2.2102$ km/s.

Table 2 summarizes the most significative parameters.

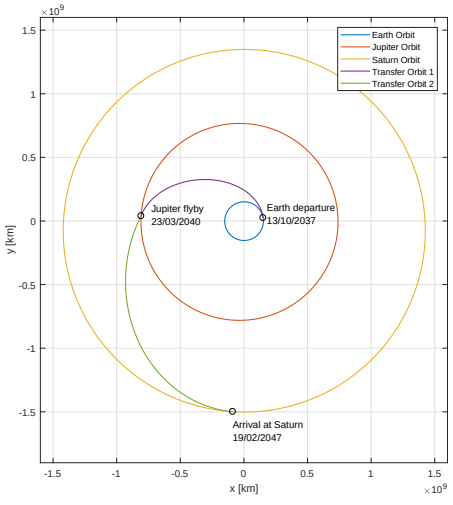

Figure 2: Second optimized trajectory

A few basic concepts can be extrapolated from the previous examples. First of all, when implementing a global optimization technique we obtain the best result in terms of total $\Delta\boldsymbol{v}$, but it is not possible to control each one of the terms that add up to the total impulse: this results in a quite high $\Delta\boldsymbol{v}_{fb}$, which would require a considerable fuel consumption. When optimizing the global $\Delta\boldsymbol{v}$ the algorithm stabilizes on a solution that is very close to performing two Homann's transfer orbits, with the true anomaly θ going from values close to 0 at departure time to values close to π when approaching the destination: this is only feasible with the additional degree of freedom given by the maneuver at the pericenter of the flyby orbit. In the second case, the flyby maneuver is reduced to near-zero value resulting in a free flyby; as a consequence, there is no *a priori* control over $\Delta\boldsymbol{v}_{launch}$ and $\boldsymbol{v}_{\infty,S}$. As far as the first term is concerned, the user will need to prune the solutions in order to find those that grant a $\Delta\boldsymbol{v}_{launch}$ compatible with available launcher technology. The $\boldsymbol{v}_{\infty,S}$ usually falls in the range $[2, 3]$ km/s, depending on the real positions of departure and arrival due to the planets' ellipticity. The maneuver

[2]The perigee argument of the flyby orbit is to be intended as the angle measured from Jupiter's transversal velocity component and the position of the pericenter of the hyperbolic flyby orbit.

DOI: 10.13009/EUCASS2019-510

in Jupiter apparently looks beneficial for the final encounter with Saturn, lowering the hyperbolic excess velocity to $\boldsymbol{v}_{\infty,S} = 1.4245$ km/s, which is better than what can usually be accomplished with a pure flyby, but still suffers the high costs required by the maneuver. Tests were run to try to find the solution with the lowest hyperbolic excess speed at Saturn's sphere of influence; the best results obtained were around $\boldsymbol{v}_{\infty,S} = 1.3$ km/s, at the expenses of more intense maneuvers in the other phases of the mission: this means that, in order to reduce the relative velocity at the encounter with Saturn, other strategies need to be implemented.

2. Optimizing the Capture with Low Thrust

In this section the results of the analysis conducted up to this point will be summarized and perfected. The Cassini Mission reached Saturn with a hyperbolic excess speed of $\boldsymbol{v}_\infty = 5.6$ km/s and, to have the spacecraft captured in the sphere of influence of the planet, a $\Delta v = 622$ m/s was necessary; this required a consumption of 800 kg of propellant,[1] which had a severe impact on the mass budget of the mission. Moreover, the spacecraft was put onto a highly elliptic orbit around Saturn, and several subsequent flybys of Saturn's moons were necessary to lower the semimajor axis of the orbit and to circularize it.[2]

Since the energy of the hyperbolic orbit entering Saturn's sphere of influence is directly proportional to the parameter $c_3 = \boldsymbol{v}_\infty^2$, reducing the relative speed means facilitating the capture maneuver. In order to do, a *low-thrusted arc* will be inserted in the transfer orbit from Jupiter to Saturn: the low thrust will be provided by an electric thruster; the main parameters involved will be:

- the acceleration α provided by the thruster
- the orientation angle β of the thrust vector
- the time during which the thruster is turned on T_{thr}
- the delay time δ to be waited from the departure from Jupiter before turning on the thruster

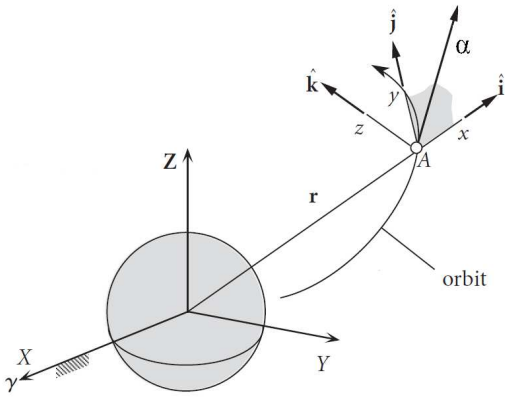

Figure 3: Comoving orbital frame of reference

The parameters will be chosen according to the performances of different types of electric thrusters available on the market (ion thrusters, Hall-effect thrusters...) based on the best fitting parameters obtained by the simulations.

2.1 Dimensionless Gaussian Planetary Equations

The method implemented to integrate the motion of the spacecraft along the thrusted arc will be integrating the *Gaussian Planetary Equations* (GPE). It is necessary to point out that applying a thrusted arc for an extended period of time makes it impossible to work with classical Keplerian orbits: the spacecraft is subject to non-conservative forces (the thrust) and Keplerian theory does not apply. During its motion along the thrusted arc the spacecraft will occupy, at each instant, a specific position in space $\vec{\boldsymbol{r}}$ with a certain velocity $\vec{\boldsymbol{v}}$; knowing the state vector allows to calculate the Keplerian parameters of the S/C *in that specific instant*: the *osculating parameters* which correspond to the *osculating orbit*.

Most of the Keplerian parameters involved in the GPE are dimensionless, others, like the semimajor axis a, are not. The calculations would require several operations between dimensionless parameters, usually close to unit value, and parameters with values that are several orders of magnitude higher than unity (all the parameters that express a length). The best way to approach the integration is therefore by using dimensionless variables: from now on, plain variables will be intended as dimensionless, while variables with a hat will represent variables with the respective dimensions. The procedure follows from the selection of a scale length a_0:

- length: $a_0 = L \Longrightarrow \hat{a} = a_0 a$
- time: $\omega_0 = \sqrt{\frac{\mu}{a_0}} \Longrightarrow \tau = \omega_0 \hat{t}$
- velocity: $v_0 = a_0 \omega_0 \Longrightarrow \hat{v} = v_0 v$
- acceleration: $\alpha_0 = a_0 \omega_0^2 \Longrightarrow \hat{\alpha} = \alpha_0 \alpha$

DOI: 10.13009/EUCASS2019-510

- angular moment: $\hat{h} = a_0^2 \omega_0 h$

Dimensionless parameters like e and θ will be left unchanged. We introduce the dimensionless parameter χ:

$$\chi = 1 + e\cos\theta = \frac{p}{r}$$

and point out the relation $h = \sqrt{p}$, that can be proved by:

$$\frac{\hat{h}^2}{\mu} = \hat{p} \Longrightarrow \frac{a_0^4 \omega_0^2}{\mu} h = a_0 p \Longrightarrow h = \sqrt{p}$$

With these considerations, the dimensionless GPE assume the form:

$$\begin{aligned}
\frac{\mathrm{d}\Omega}{\mathrm{d}\tau} &= \frac{\sqrt{p}}{\chi}\frac{\sin(\theta+\omega)}{\sin i}\alpha_z \\
\frac{\mathrm{d}\omega}{\mathrm{d}\tau} &= \frac{\sqrt{p}}{e}\left\{-\cos\theta\alpha_x + \left(1+\frac{1}{\chi}\right)\sin\theta\alpha_y - \frac{e}{\chi}\cot i \sin(\theta+\omega)\alpha_z\right\} \\
\frac{\mathrm{d}i}{\mathrm{d}\tau} &= \frac{\sqrt{p}}{\chi}\cos(\theta+\omega)\alpha_z \\
\frac{\mathrm{d}a}{\mathrm{d}\tau} &= \frac{2a^2}{\sqrt{p}}\left\{e\sin\theta\alpha_x + \chi\alpha_y\right\} \\
\frac{\mathrm{d}e}{\mathrm{d}\tau} &= \sqrt{p}\left\{\sin\theta\alpha_x + \left[\left(1+\frac{1}{\chi}\right)\cos\theta + \frac{e}{\chi}\right]\alpha_y\right\} \\
\frac{\mathrm{d}\theta}{\mathrm{d}\tau} &= \frac{\chi^2}{p^{3/2}} + \frac{\sqrt{p}}{e}\left\{\cos\theta\alpha_x - \left(1+\frac{1}{\chi}\right)\sin\theta\alpha_y\right\}
\end{aligned}$$

In these equations $(\alpha_x, \alpha_y, \alpha_z)$ are the components of the nondimensional thrust acceleration in the orbital frame (see figure 3). The orbital frame moves with the satellite, with the x axis along the orbital radius and the z axis parallel to the angular momentum. Those components are:

$$\begin{cases} \alpha_x = \alpha\sin\beta \\ \alpha_y = \alpha\cos\beta \\ \alpha_z = 0 \end{cases}$$

At this point, a few last steps can be taken to simplify the equations. First of all, in the hypothesis of working with planar orbits, there will be no need to provide an out-of-plane component of the acceleration, which implies $\alpha_z = 0$ eliminating a few of the terms. It can be noticed that both the parameters Ω and i depend entirely on α_z: this means that the first two equations can be removed from the computation, since the two parameters involved do not play any role. It will prove to be convenient to work with two alternate parameters: the longitude $l = \theta + \omega$ will be substituted to ω and the semiparameter $p = a(1-e^2)$ will be substituted to e. While the derivative of the longitude can be calculated adding the two GPE for θ and ω, the derivative of the semiparameter needs to be calculated through the chain rule:

$$\frac{\mathrm{d}p}{\mathrm{d}\tau} = \frac{\mathrm{d}a}{\mathrm{d}\tau}\left(1-e^2\right) - 2ae\frac{\mathrm{d}e}{\mathrm{d}\tau}$$

For each step of the integration the eccentricity can be derived from a and p: $e = \sqrt{1-\frac{p}{a}}$. We finally get to the final form of the four GPE that will be used to describe the dynamics:

$$\begin{aligned}
\frac{\mathrm{d}a}{\mathrm{d}\tau} &= \frac{2a^2}{\sqrt{p}}\left\{e\sin\theta\alpha_x + \chi\alpha_y\right\} \\
\frac{\mathrm{d}p}{\mathrm{d}\tau} &= 2\frac{p^{3/2}}{\chi}\alpha_y \\
\frac{\mathrm{d}\theta}{\mathrm{d}\tau} &= \frac{\chi^2}{p^{3/2}} + \frac{\sqrt{p}}{e}\left\{\cos\theta\alpha_x - \left(1+\frac{1}{\chi}\right)\sin\theta\alpha_y\right\} \\
\frac{\mathrm{d}l}{\mathrm{d}\tau} &= \frac{\chi^2}{p^{3/2}}
\end{aligned}$$

DOI: 10.13009/EUCASS2019-510

Table 3: Transfer orbit

Transfer orbit			
e	0.455335	a	0.6873765
i	0.0	$\theta_{departure}$ (rad)	1.546061
ω (deg)	88.6728	$\theta_{arrival}$ (rad)	3.112125
Ω	/	ΔT	1.365526

From the point of view of the analysis the values of the Keplerian elements (a_f, p_f) of the final osculating orbit play an important role. In fact, we will use the following dimensionless version of them:

$$\xi = \frac{a_f}{a_S}, \qquad \eta = \frac{p_f}{a_S} \tag{1}$$

where a_S is the semimajor axis of the Saturn's orbit.

In this analysis there is a curve in the plane (ξ, η) — the Γ curve— that plays a very important role.

$$\Gamma : 2 - \frac{1}{\xi} - \eta = 0$$

This curve is the locus of points that correspond to an orbit that has its apogee on Saturn's orbit; all the points below the curve correspond to orbits that intersect Saturn's orbit, while those lying above correspond to orbits that do not.

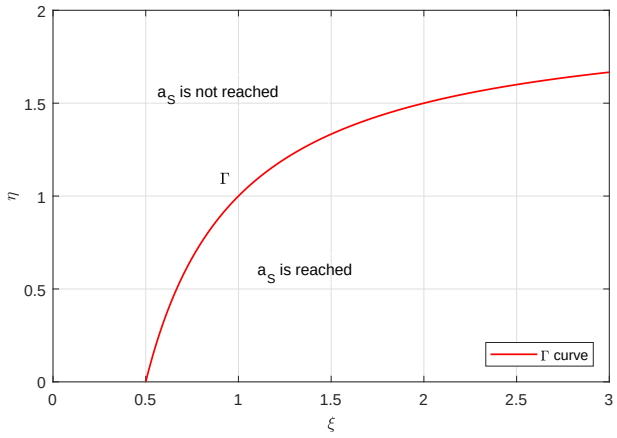

Figure 4: The Γ curve for planets circular orbits

3. Implementation and Results

In this section we will summarize the results obtained in our analysis applying the same optimization technique described in other communication of our group.[20] **The basic rule used in the optimization process is as follows: in each point of the trajectory the angle β is selected in such a way that the final hyperbolic excess velocity at arrival to Saturn is decreased**. For the sake of brevity the details of the optimization process will be omitted. The interested reader can found the complete analysis in.[18]

The orbital design considered involves a free flyby around Jupiter; the parameter chosen as length scale is the heliocentric radius of the intersection point between Saturn and the transfer orbit: $a_0 = \hat{r}$. This choice proves to be efficient because it reduces all length quantities to values lower than 1, and with $r = 1$ the parameters (ξ, η) and (ϕ, ψ) result numerically equal to the dimensionless values of (a_f, p_f) and (a_S, p_S) respectively, avoiding additional manipulation. The Gaussian Planetary Equations will be solved using MATLAB®/ Simulink implementing the Runge-Kutta(4,5) method (ode45). In the simulation, the thrust appears in the form of a square wave with amplitude equal to the acceleration in the time interval while the thruster is on, and equal to zero when turned off; the simulation terminates when the orbital radius of the transfer orbit reaches $r = 1$. The dimensionless parameters of the transfer orbit are summarized in table 3.

As mentioned previously, there are four main design drivers in the optimization process: α, β, T_{thr} and δ. The angle β can be derived from the optimal control law,

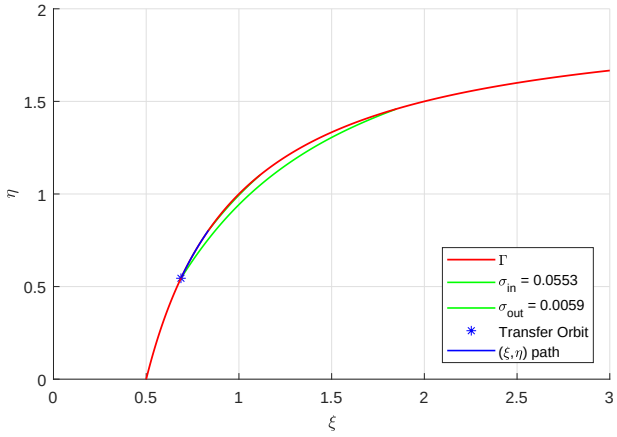

Figure 5: Evolution along the (ξ, η) plane with $\alpha = 0.3$ and $T_{thr} = 5$ years

DOI: 10.13009/EUCASS2019-510

and is therefore defined in every circumstance. This angle is independent from the acceleration α provided: intuitively, this means that the acceleration does not affect the path that joins different points on the (ξ,η) plane, but only the time it requires the thruster to cover that path. In each of the analyses presented the angle β was calculated in order to reach tangency condition first, at to move along the Γ curve subsequently. Figure 5 shows an example of the evolution of the transfer orbit in the (ξ,η) plane.

Optimal choices for α, T_{thr} and δ: Several simulations were run with a variety of values for each parameter: the purpose is to identify significant correlations among the parameters and optimal values for the implementation of the method that are not evident from a first mathematical analysis. The test values for the acceleration are $\alpha \in [0.2, 0.4]$ which correspond, for a spacecraft with a mass of 1000 kg, to a thrust that falls in the range $F \in [10, 25]$ mN; these values were chosen based on the performances of a variety of ion thrusters and hall effect thrusters currently available on the market[14] so that the thruster's power requirement would not exceed the indicative value of 400 W, which can be provided through RTG's. The values for T_{thr} correspond to several years of activity, as electric thrusters usually have a life expectancy of above 2 years.[11] Hypothetically, should a thruster require a T_{thr} longer than its own estimated life, more thrusters can be utilized in sequence to provide thrust when the firs one(s) cease to function, as electric thrusters have a very low impact on the mass budget of the mission.

In what follows we present three runs of simulations:

- simulations with constant T_{thr}
- simulations with constant α
- simulations with optimal values of δ (in the next section)

Simulations with constant T_{thr}. Several simulations were run assuming **a constant value for $T_{thr} = 2.5$ years**. The independent variable in the plots is the delay time δ; curves are given for different values of α.

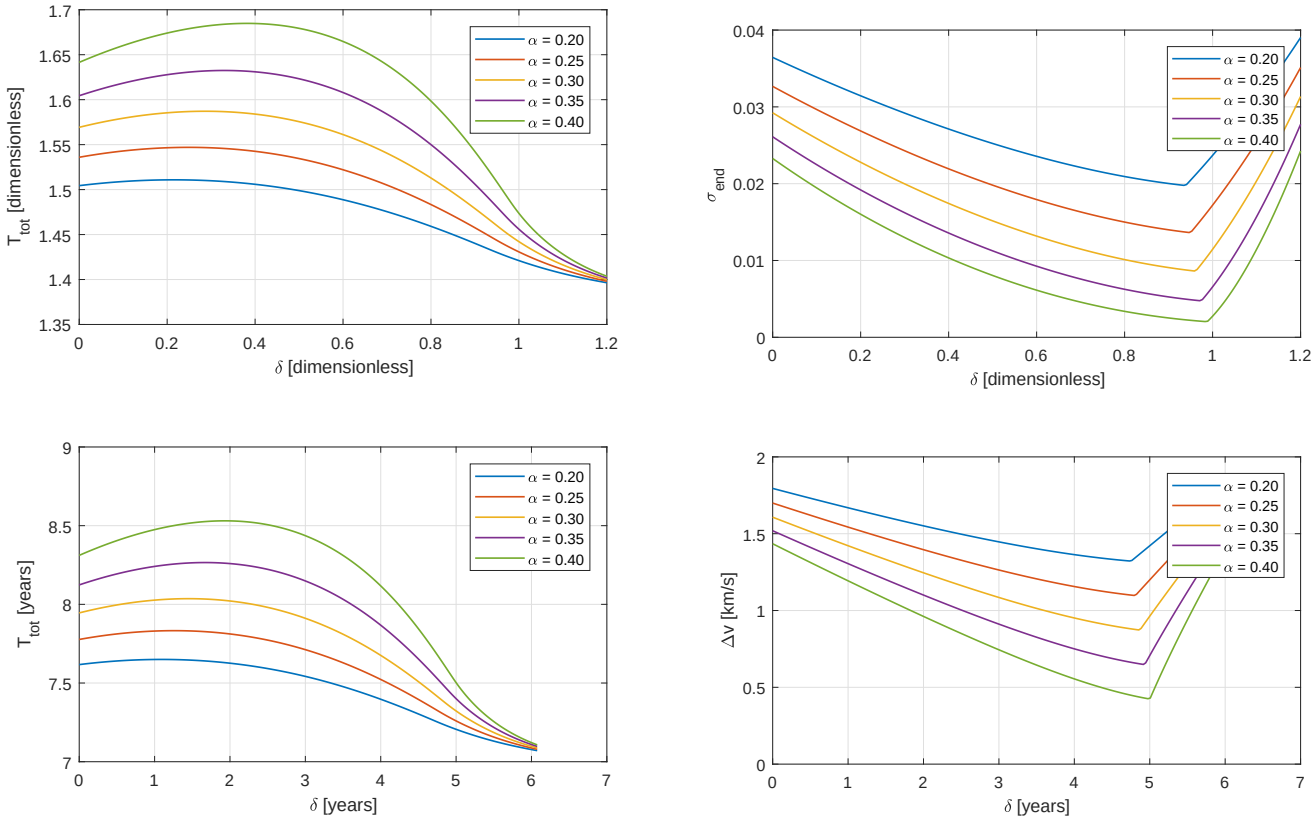

Figure 6: (Left): Total time of flight for different values of δ and α. (Right): v_∞ for different values of δ and α

As it can be seen from the graphs a higher thrust results in a much lower relative speed at the encounter. As a downside, a higher thrust implies a higher total flight time, as it can be visualized in fig. 6 (left part). There is an

DOI: 10.13009/EUCASS2019-510

optimal choice for the delay time δ. In effect, looking at fig. 6 (right part), it can be noted that **the minimum relative velocity for each curve is reached when the thruster is turned on exactly 2.5 years before the end of the total fight time**. This means that the optimal position for the thrusted arc is at the exact end of the transfer orbit.

Simulations with constant α. In this second set of simulations, the acceleration parameter has been kept constant to $\alpha = 0.3$, while the time of thrust T_{thr} is the parameter that changes in the different curves. Again the independent variable is the delay time δ.

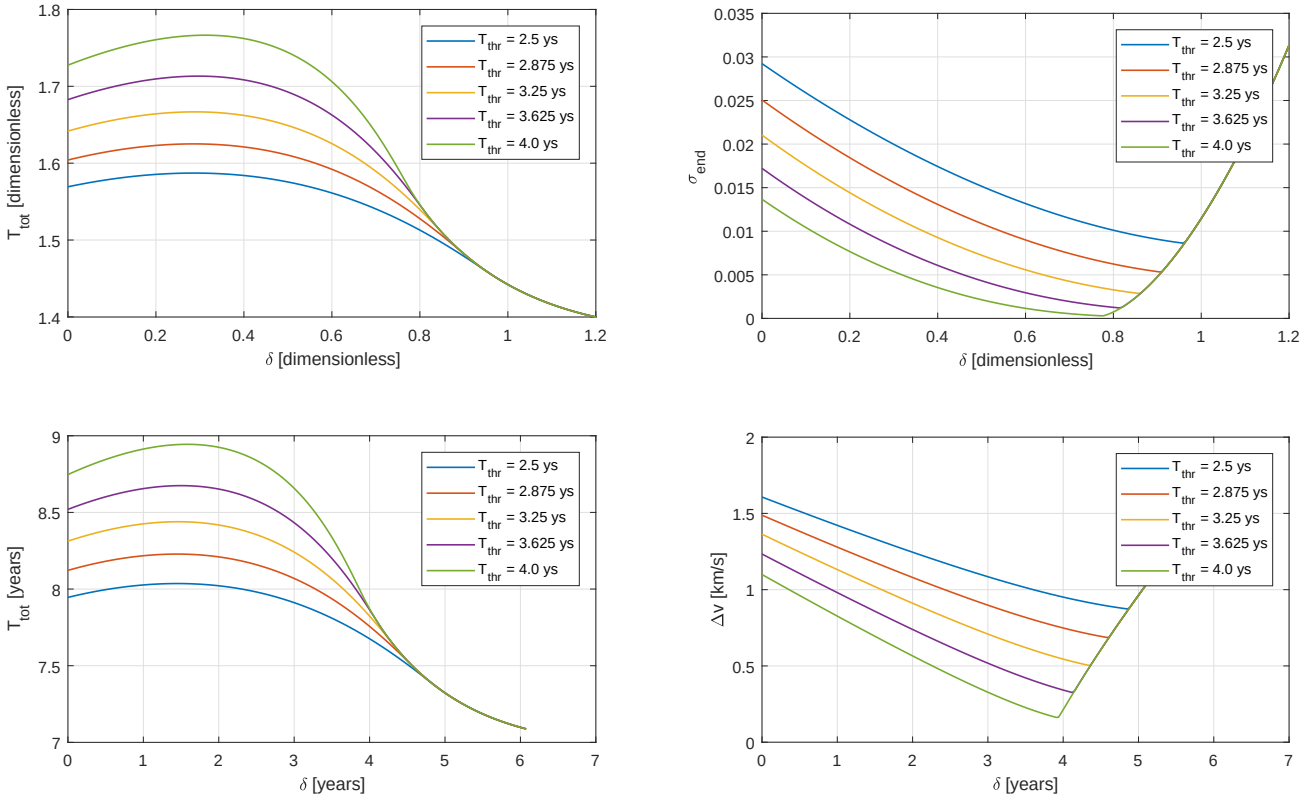

Figure 7: (Left): Total time of flight for different values of δ and T_{thr}. (Right): v_∞ for different values of δ and T_{thr}

In this case as well, the behavior of the curves is qualitatively similar: increasing T_{thr} allows to reduce the v_∞, at the expenses of a higher total flight time, as it can be seen in fig. 7 (left part). Once more, looking at fig. 7 (right part) the optimal value for the delay δ appears to be the one consisting in placing the thrusted arc at the exact end of the transfer orbit. One interesting observation about these last charts is the fact that for values of δ sufficiently high, the curves at different T_{thr} overlap: this makes sense because when the thruster is turned on, for example, 2.5 years before reaching Saturn's altitude, the integration is not affected by how long the thruster can keep working, and will stop once the condition $r = 1$ is reached, regardless of how long the thruster could hypothetically keep working.

4. Simulations with optimal δ values

The analysis of the previous section shows that:

- the optimal location of the thrusted arc is at the end of the transfer orbit, regardless of the other parameters involved
- for each pair of values of (α, T_{thr}) there is an optimal value of δ , namely $\delta^*(\alpha, T_{thr})$, for which the v_∞ is minimum

In this section the degree of freedom associated with δ is removed. Thus, for each combination of parameters (α, T_{thr}), the value of δ considered is

$$\delta = \delta^*(\alpha, T_{thr})$$

DOI: 10.13009/EUCASS2019-510

Table 4: Parameters of the regression line (all data points)

	m	q	R^2	$T_{thr,max}$ (ys)
$\alpha = 0.20$	-0.32317	2.13741	0.99834	6.614
$\alpha = 0.25$	-0.41143	2.13307	0.99903	5.185
$\alpha = 0.30$	-0.51230	2.15437	0.99957	4.205
$\alpha = 0.35$	-0.60861	2.16363	0.99975	3.555
$\alpha = 0.40$	-0.70551	2.17328	0.99989	3.080

in order to reach the minimum v_∞ of each curve. The curves provide the relative velocity v_∞ as function of the thrust time, for different values of the acceleration, and can be visualized in fig. 8.

The curves are not drawn for the entire domain as the variable T_{thr} needed to be discretized due to the high non-linearity of the problem and the insurgence of some numerical instability around $v_\infty \to 0$.

Figure 8 shows that v_∞ appears to have a quasi-linear dependance from the time of thrust T_{thr}. A regression analysis is conducted to verify the accuracy with which the curves could be approximated by a straight line having the equation:

$$v_\infty = m \cdot T_{thr} + q$$

The parameter R^2 visualized in the table 4 is called coefficient of determination and represents the reliability with which the actual curve can be approximated by the regression line: the best result is obtained when $R^2 = 1$. Moreover, from the equation of the regression line, we can extrapolate the value of $T_{thr,max}$, which is the time of thrust that needs to be provided to, hypothetically, reach the best condition $v_\infty = 0$.

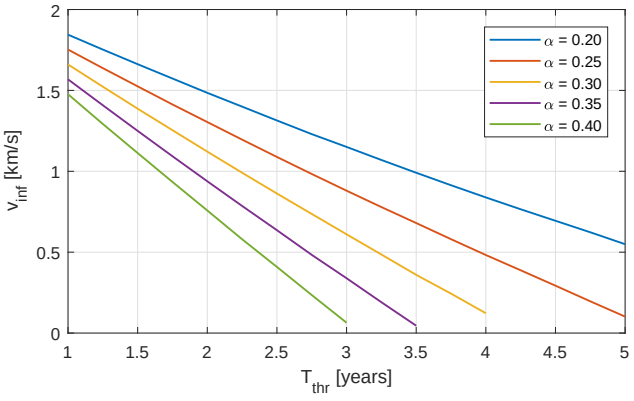

Figure 8: v_∞ as function of T_{thr} for different values of α

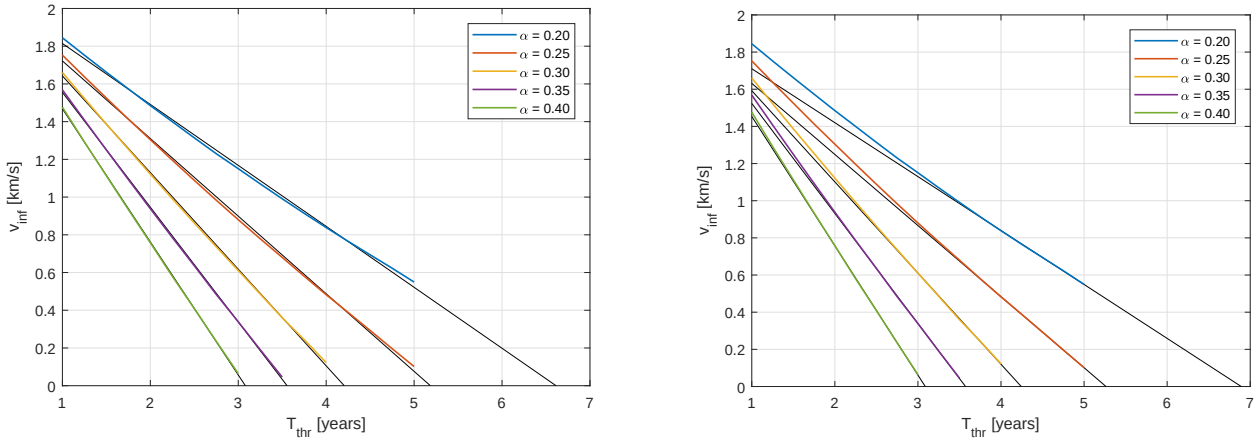

Figure 9: (Left): Regression line (all data points). (Right): Regression line (last 5 data points).

As it can be visualized in fig. 9 (left part), there is a better concurrence between curve and regression line for higher values of α, but only because they were calculated for a smaller number of data points closer to the respective value of $T_{thr,max}$. A better estimate can be calculated utilizing, for each curve, only the last five data points, obtaining a regression line that approximates the slope of the curve at its final end (fig. 9 right part). New simulations were run adopting, for each value of the acceleration, the $T_{thr,max}$ values extrapolated from fig. 9 (right part): the results are visualized in fig. 10, where the v_∞ is plotted versus the delay time δ. The best results, expressed in the table 6, show that the v_∞ has been reduced by an additional order of magnitude, down to values of 10 m/s. The results calculated from the extrapolated data for $T_{thr,max}$ do not produce $v_\infty = 0$ yet, meaning that there are errors that are implicit within the

DOI: 10.13009/EUCASS2019-510

Table 5: Parameters of the regression line (last 5 data points)

	m	q	R^2	$T_{thr,max}$ (ys)
$\alpha = 0.20$	-0.29024	2.00037	0.99991	6.892
$\alpha = 0.25$	-0.38258	2.01401	0.99998	5.264
$\alpha = 0.30$	-0.49077	2.08275	0.99980	4.244
$\alpha = 0.35$	-0.59212	2.11564	0.99993	3.573
$\alpha = 0.40$	-0.69587	2.14922	0.99995	3.089

Table 6: v_∞ versus δ with optimal value for T_{max}

	$T_{thr,max}$ (ys)	$v_{\infty,min}$ (m/s)
$\alpha = 0.20$	6.892	59.50
$\alpha = 0.25$	5.264	11.83
$\alpha = 0.30$	4.244	11.72
$\alpha = 0.35$	3.573	11.68
$\alpha = 0.40$	3.089	11.67

approximation, but with further iterations and more data points an exact final result could theoretically be calculated. Nevertheless, the results provided are already very good in the perspective of minimizing the relative velocity, and are only affected by the limitations given by the life expectancy of real electric thrusters.

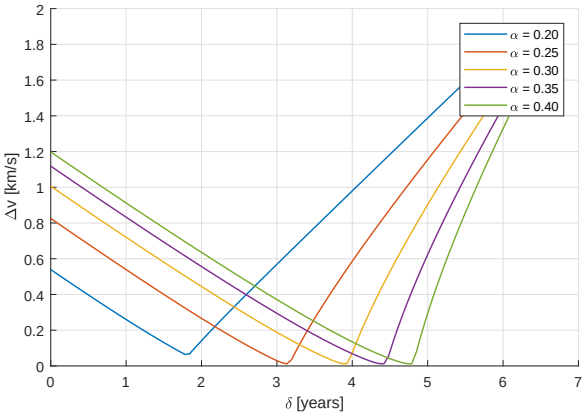

Figure 10: v_∞ versus δ with optimal value for T_{max}

5. Orbital Design of the Mission

In this section the theory and the results developed so far will be used to obtain a preliminar design of a mission to Saturn. The parameters selected for this initial design will not be speculative, but chosen from state-of-the-art pieces of technology to evaluate the feasibility of the mission and its cost/outcome ratio. *The total mass of the spacecraft will be assumed to be 1000 kg, while the initial orbital design will be that presented in table 3 involving a pure flyby around Jupiter.*

As part of this initial design, appropriate values should be selected for the parameters α and T_{thr}. The best way to provide for the thruster's and the satellite's power needs throughout the mission is given by *Radioisotope Thermoelectrical Generators (RTG's)*. Assuming to install two RTG's to supply for the thruster and the satellite's other needs, a good choice would imply a power requirement of 300-400 W maximum. The models of RTG's used in both the Galileo and Cassini missions would be sufficient for this mission. The appropriate thruster needs therefore to be picked in order to require a total power consumption that matches the capabilities of the RTG's. An interesting and newer model is the PPS®X00 currently being developed at Safran: this Hall thruster is being designed to work

DOI: 10.13009/EUCASS2019-510

Table 7: Transfer orbit from Jupiter to Saturn

Transfer orbit			
Jupiter Flyby	08/03/2040	Arrival at Saturn	26/08/2047
e	0.455335	a (km)	1.0319469e+09
i	0.0	$\theta_{departure}$ (rad)	1.545474
ω (deg)	87.4732	ΔT (ys)	7.47279

within the power range of [200,1000] W to meet a variety of performance requirements; the optimal design point is at 650 W, providing 40 mN of thrust with an efficiency equal to that of the best state-of-the-art models available.[16] The PPS®X00 is expected to be available on the market by 2020.[16]

From the operating envelope of this thruster it is possible to obtain an estimate of the thrust available with our problem constraints. This thruster can be used for the mission, with a power input of 300 W, a thrust output of 19 mN and a specific impulse of 1150 s, as we are interested in maximizing the thrust. *This leads to the definition of the acceleration* $\alpha = 0.3228$*, which falls in the range of parameters previously investigated. As for the choice of* T_{thr} *we assume to use only one thruster, therefore a total functioning time of 2.5 years*[7].

For the sake of brevity we omit here the selection of the launch windows and other details that, if desired, can be consulted in the reference.[18] We present the final orbit obtained from the theory carried out in the previous pages. The parameters of the transfer orbit from Jupiter to Saturn are summarized in table 7.

The thruster is turned on after $\delta = 0.98139 = 4.97065$ years: with the engine working continuously for 2.5 years.The final trajectory can be visualized in fig. 11, where the green transfer trajectory is the hypothetical solution to Lambert's problem than connects Jupiter and Saturn in the same time, but without the thrusted arc.

The orbit with the thrusted arc offers a better solution to the problem of approaching Saturn, as it can be seen from the figure, because it is tangent to Saturn's orbit at the intersection point, while the normal transfer orbit is not. The orbit in green reaches Saturn with $v_\infty = 2.12135$ km/s, while with the final design for the thrusted orbit the hyperbolic excess speed is reduced to:

$$v_\infty \approx 0.757 \text{ km/s}$$

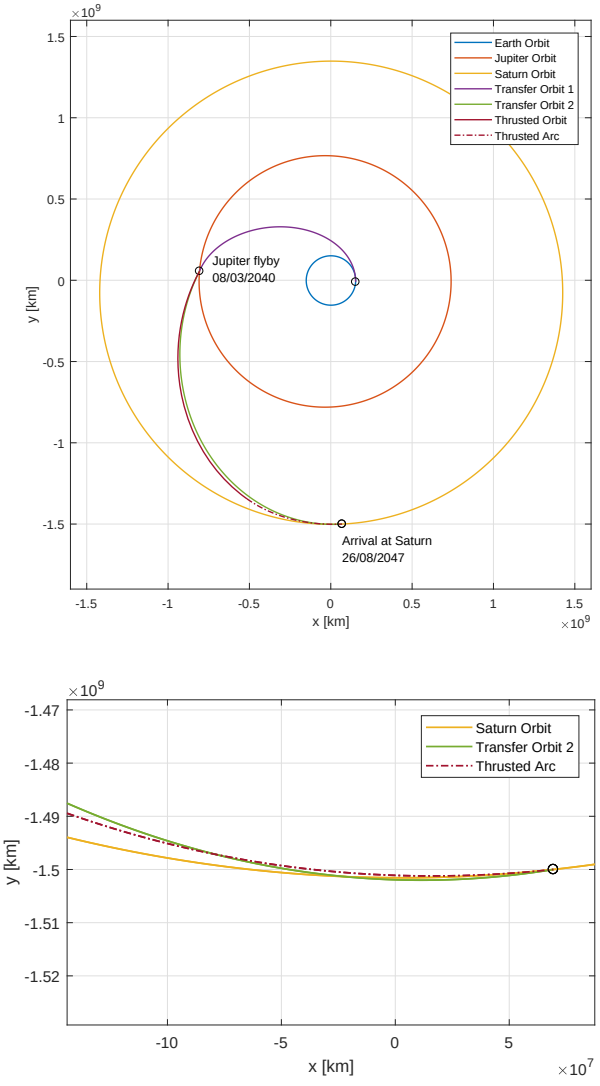

Figure 11: Final transfer orbit with thrusted arc

6. Capture

In the previous sections, the aim was to reduce the relative speed between the spacecraft and Saturn at the encounter. In this section we want to describe, very succinctly, de real benefits of this design, which consist in easing the capture procedure of the spacecraft into Saturn's gravity field. To avoid further propellant consumption the capture will be performed by a bare electrodynamic tether (EDT); the study of feasibility carried out in the following pages will follow the procedures outlined by E. C. Lorenzini and J. R. Sanmartín in references.[6,8–10,17]

The current induced on the tether is the so called orbital-motion-limited current I_{OML}. This current is limited the tether's short circuit value $\sigma_c E_m A$ and is a function of a characteristic length L_{ch}, which gauges ohmic effects on the

DOI: 10.13009/EUCASS2019-510

bare tether.[10] The expression for L_{ch} is:[10]

$$\frac{4}{3} e N_e \frac{p L_{ch}}{\pi} \sqrt{\frac{2 e E_m L_{ch}}{m_e}} = \sigma_c E_m A$$

where the following terms are involved: i) e, m_e, N_e: electron charge, mass and density in the plasma environment respectively, ii) p: perimeter of the tether, iii) A: cross section of the tether, and iv) σ_c: electric conductivity of the tether.

Since it is more convenient to obtain lower values for L_{ch}, the preferable shape of the tether is that of a tape of width w and thickness h, to reduce the ratio A/p. For a thickness h that's negligible compared to the width, the expression above reduces to:[17]

$$\frac{4}{3} e N_e \frac{2 w L_{ch}}{\pi} \sqrt{\frac{2 e E_m L_{ch}}{m_e}} = \sigma_c E_m w h \Longrightarrow L_{ch} \propto \frac{h^{2/3} E_m^{1/3}}{N_e^{2/3}}$$

The I_{OML} current can be calculated through a length-averaged current value i_{av}:[17]

$$\frac{I_{OML}}{\sigma_c E_m w h} = i_{av}\left(\frac{L}{L_{ch}}\right)$$

where small i_{av} correspond to negligible ohmic effects and $i_{av} \approx 1$ to dominant ohmic effects. The value of i_{av} is a function of L/L_{ch}, with L being the actual tether length

The capture operation performed by an ET strongly depends on the planetary space environment, namely on the magnetic field $\vec{\boldsymbol{B}}$ and the electron density of the ambient plasma N_e. The magnetic field $\vec{\boldsymbol{B}}$ in Saturn es well known. However, the plasma environment around Saturn in extremely diverse and articulated: it is therefore complicated to provide a model that describes N_e with precision. The most detailed and up-to-date information of Saturn's plasma ambient come from the observations of the spacecraft Cassini.[5] Fortunately, the data permit to assure that the values of the averaged current i_{av} will be close to unity for a wide range of plasma densities.

In order to effectively perform a planetary capture, the Lorentz drag needs to be able to perform a work $|W_d|$ to reduce the eccentricity from a hyperbolic value $e_h > 1$ to an elliptic value $e_e < 1$. This work is:

$$|W_d| = M_{S/C} \frac{v_\infty^2}{2} \cdot \frac{e_h - e_e}{e_h - 1} \Rightarrow \frac{|W_d|}{m_t v_\infty^2/2} = \frac{M_{S/C}}{m_t} \cdot \frac{e_h - e_e}{e_h - 1}$$

The rearranged expression on the right hand side is particularly useful because it reduces the problem to a limited number of dimensionless coefficients:

- $\frac{M_{S/C}}{m_t}$: it is the ratio between the spacecraft's mass and the tether mass;
- $\frac{e_h - e_e}{e_h - 1}$: it depends on the eccentricities before and after the dragged arc; e_h is usually known and very close to 1: $e_h - 1 \to 0$;
- $\frac{|W_d|}{m_t v_\infty^2/2}$: it is the dimensionless drag work, and summarizes all the dynamic effects of the drag force on the spacecraft's trajectory.

The work $|W_d|$ takes the following nondimensional value W_d^*, for a retrograde orbit:

$$W_d^* = 2 {r_M^*}^{8/3} \int_1^\infty \frac{(r_M^* + r^*) dr^*}{{r^*}^6 \sqrt{r^* - 1}} \cdot < i_{av} >$$

Assuming the periapse to be very close to the surface of Saturn and the hyperbolic excess speed to be that of a non-thrusted transfer orbit after a Jupiter flyby ($r_P \approx R_S$ and $v_\infty \approx 2.5$) leads to:

$$\frac{e_h - e_e}{e_h - 1} \cdot \frac{M_{S/C}}{m_t} =< i_{av} > \cdot 6.13$$

At periapse, the characteristic length is $L_{ch} \approx 26$ km; designing the tether to be 52 km long leads to $i_{av} = 0.5$ at periapse, where the magnetic field is at its strongest value. Assuming also, as in first approximation, that the final orbit be exactly parabolic ($e_e = 1$) provides:

$$\frac{M_{S/C}}{m_t} \approx 3$$

DOI: 10.13009/EUCASS2019-510

which is comparable to the values for a Jupiter application.[17] For a spacecraft mass of 1000 kg this leads to a tether mass $m_t = 333$ kg, which in the case of aluminium provides $w = 24$ cm for $h = 10^{-2}$ mm.

We want now to analyse the possible benefits of reducing the hyperbolic excess speed in comparison to the results that have previously been calculated in:[17] the dependance from v_∞ is clear in the expression for B_s^{*2}. A lower v_∞ results in a value for the eccentricity that will be closer to unity; specifically, maintaining in both cases the hypothesis $r_P \approx R_S$ we obtain $e_h^I = 1.009930$ for $v_\infty^I = 2.5$ km/s and $e_h^{II} = 1.001589$ for $v_\infty^{II} = 1$ km/s. The reference value $v_\infty = 1$ km/s has been chosen for a conservative analysis, even though the relative speed, as has been shown previously, can be deduced to a lower value. We assume that none of the parameters involved change besides the dimensions of the tether l and w: as a result of this assumption, the characteristic length L_{ch} stays unchanged as well as the result of the integral in the expression for W_d^*, which was calculated with the hypothesis of the orbits being parabolic.

Reducing the tether mass, m_t is definitely of great interest for the entire mission: assuming to have a constant space mass $M_{S/C}$ in both cases, a lower tether mass allows a higher mass fraction to be utilized for payload. The two parameters that are object of the optimization are **length and width**; the thickness is kept constant as well as the material density. The calculations from previous sections remain valid, providing a characteristic length of $L_{ch} = 26$ km at periapse. We want the tether to be at most as long as it is in the first case analyzed (52 km), but preferably shorter to be in the range where the i_{av} current is a linear function of the ratio L/L_{ch}, which in the case of a constant characteristic length translates into $i_{av} \propto l$. In this analysis we assume that the final orbit be barely elliptical ($e_e \to 1$) so that the eccentricity ratios equal 1. These considerations result in:

$$\frac{m_t^I}{m_t^{II}} = \kappa \cdot \frac{l^{II}}{l^I}$$

where $\kappa = 6.25$ is the squared ratio between the hyperbolic excess speeds in the first and second case:

$$\kappa = \left(\frac{v_\infty^{II}}{v_\infty^I}\right)^2$$

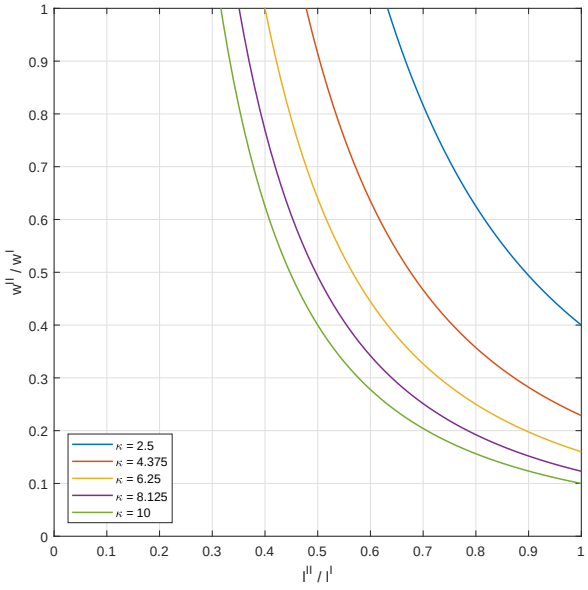

Figure 12: w^{II}/w^I versus l^{II}/l^I for different κ values

Expressing the tether mass as $m_t = \rho lwh$ leads to the ultimate:

$$\kappa \frac{w^{II}}{w^I}\left(\frac{l^{II}}{l^I}\right)^2 = 1$$

which can be interpreted as follows: in the case with a reduced hyperbolic excess velocity, the capture is performed equivalently by an electrodynamic tether that is κ times narrower ($w^I = \kappa w^{II}$) or $\sqrt{\kappa}$ times shorter ($l^I = \sqrt{\kappa} l^{II}$). Combination of the two are also possible, reducing both the dimensions, following the plots in fig. 12 obtained reformulating the last equation.

With the mass m_t being directly proportional to both w and l, the best solution to reduce the total tether mass would be that consisting in leaving the length unchanged and reducing the width by a factor κ. Unfortunately, with the tether width being of the order of magnitude of centimeters, it might not be safe to scale it down so much without risking the rupture of the tether. In this circumstance, the width can be reduced to the minimum safe value, while a fraction of κ can be 'implemented' in a reduction of the tether length l.

7. Conclusion and future works

This paper present the initial design of a tether mission to Saturn. It is important to highlight the following aspects of the mission that is proposed:

- it is a small mission involving a global mass of the order of 1000 kg, much lower than the mass of the S/C of the Cassini/Huygens.

DOI: 10.13009/EUCASS2019-510

- it considers a flyby around Jupiter
- it incorporates a low thrust engine which provides a thruster arc *in the final part of the trajectory*. This thrusted arc permit to decrease the hyperbolic excess velocity $\boldsymbol{v}_{\infty,S}$ at arrival to Saturn to values lower than 1 km/s
- the capture is carried out by a bare electrodynamic tether. The low values of $\boldsymbol{v}_{\infty,S}$ allow improve the design of the tether reducing, basically, its mass, and making room for bigger payloads.

Obviously there are many aspects that must be considered in an interplanetary mission like this one. In the future many parts of this analysis will be improved and modified in order to get a more solid and well-founded proposal.

One of the future works is to improve the tether design, if possible, to visit some moons of the Saturn following the trail of the analysis performed in.[22]

8. Acknowledgments

The work of E. Fantino and J. Peláez has been supported by Khalifa University of Science and Technology's internal grants FSU-2018-07 and CIRA-2018-85. These authors also acknowledge the support provided by the project entitled Dynamical Analysis of Complex Interplanetary Missions with reference ESP2017-87271-P, supported by Spanish Agencia Estatal de Investigación (AEI) of Ministerio de Economía, Industria y Competitividad (MINECO), and by European Found of Regional Development (FEDER).

References

[1] Fernando Peralta and JC Smith Jr. Cassini trajectory design description. volume 85 of *Advances in the AAstronautical Sciences*, pages 1065–1084, 1993.

[2] Fernando Peralta and Steve Flanagan. Cassini interplanetary trajectory design. *Control Engineering Practice*, 3(11):1603–1610, 1995.

[3] Troy Goodson, Donald Gray, Yungsun Hahn, and Fernando Peralta. Cassini maneuver experience-launch and early cruise. In *Guidance, Navigation, and Control Conference and Exhibit*, 1998.

[4] Jesús Peláez. Self balanced electrodynamic tether. In *The 2004 AIAA/AAS Astrodynamics Specialist Conference and Exhibit*, AIAA paper 2004-5309, pages 1–14, 2004. 16-19 August 2004, Providence, Rhode Island, USA.

[5] AM Persoon, DA Gurnett, WS Kurth, GB Hospodarsky, JB Groene, P Canu, and MK Dougherty. Equatorial electron density measurements in saturn's inner magnetosphere. *Geophysical research letters*, 32(23), 2005.

[6] Juan R Sanmartin and Enrico C Lorenzini. Exploration of outer planets using tethers for power and propulsion. *Journal of Propulsion and Power*, 21(3):573–576, 2005.

[7] Jonathan Van Noord. Lifetime assessment of the next ion thruster. In *43rd AIAA/ASME/SAE/ASEE Joint Propulsion Conference & Exhibit*, 2007. 8-11 July, Cincinnati, OH.

[8] Juan R Sanmartin, Mario Charro, Enrico C Lorenzini, Henry B Garrett, Claudio Bombardelli, and Cristina Bramanti. Electrodynamic tether at jupiter-I: Capture operation and constraints. *IEEE Transactions on Plasma Science*, 36(5):2450–2458, 2008.

[9] Juan R Sanmartin, Mario Charro, Enrico C Lorenzini, Henry B Garrett, Claudio Bombardelli, and Cristina Bramanti. Electrodynamic tether at jupiter –ii: Fast moon tour after capture. *IEEE Transactions on Plasma Science*, 37(4):620–626, 2009.

[10] Juan Ramón Sanmartín Losada, Enrico C Lorenzini, and Manuel Martínez Sánchez. A review of electrodynamic tethers for space applications. 2009.

[11] Daniel A Herman. Nasa's evolutionary xenon thruster (next) project qualification propellant throughput milestone: Performance, erosion, and thruster service life prediction after 450 kg. 2010. NASA/TM–2010-216816.

[12] Cynthia B Phillips and Robert T Pappalardo. Europa clipper mission concept: Exploring jupiter's ocean moon. *Eos, Transactions American Geophysical Union*, 95(20):165–167, 2014.

DOI: 10.13009/EUCASS2019-510

[13] JJ Plaut, S Barabash, L Bruzzone, M Dougherty, C Erd, L Fletcher, R Gladstone, O Grasset, L Gurvits, P Hartogh, et al. Jupiter icy moons explorer (juice): Science objectives, mission and instruments. In *Lunar and Planetary Science Conference*, volume 45, page 2717, 2014.

[14] Elaine M Petro and Raymond J Sedwick. Survey of moderate-power electric propulsion systems. *Journal of Spacecraft and Rockets*, 54(3):529–541, 2017.

[15] Juan R Sanmartín, Mario Charro, Henry B Garrett, Gonzalo Sánchez-Arriaga, and Antonio Sánchez-Torres. Analysis of tether-mission concept for multiple flybys of moon europa. *Journal of Propulsion and Power*, 33:338—342, 2017.

[16] N. Cornua J. Vaudolona, V. Viala and I. Habbassib. Pps®x00 hall thruster development at safran. Bremen, Germany, October 2018. 69th International Astronautical Congress (IAC), International Astronautical Federation. Paper IAC-18-C4.4.9x45869.

[17] JR Sanmartín, J Peláez, and I Carrera-Calvo. Comparative saturn-versus-jupiter tether operation. *Journal of Geophysical Research: Space Physics*, 123(7):6026–6030, 2018.

[18] Riccardo Calaon. Preliminary design of a tethered mission to saturn. Master's thesis, Università degli Studi di Padova/Universidad Politécnica de Madrid, 2019.

[19] Jesús Peláez Elena Fantino, Roberto Flores and Virginia Raposo-Pulido. Optimization of saturn orbit insertion impulse using deep-space low thrust. *Journal of Guidance, Control, and Dynamics*, 2019. (Submitted).

[20] Roberto Flores Elena Fantino and Jesús Peláez. Design of a low-thrust assisted trajectory to saturn. 2019. 8TH EUROPEAN CONFERENCE FOR AERONAUTICS AND AEROSPACE SCIENCES (EUCASS).

[21] J. R. Sanmartín and J. Peláez. Tether capture of spacecraft at neptune. Proceedings of the 2019 International Conference on Tethers in Space, 2019. Madrid, June 12-14 2019.

[22] Juan R. Sanmartín and Jesús Peláez. Planetary exploration of saturn moons dione and enceladus. 2019. 8TH EUROPEAN CONFERENCE FOR AERONAUTICS AND AEROSPACE SCIENCES (EUCASS).